EFFICIENT ANALYSIS AND OPTIMIZATION OF REFLECTARRAY ANTENNAS FOR SATELLITE TELECOMMUNICATION MISSIONS

Daniel R. Prado[1], Manuel Arrebola[2], Jesús A. López-Fernández[2], Marcos R. Pino[2], George Goussetis[1], and José A. Encinar[3]

[1]*Institute of Sensors, Signals and Systems, School of Engineering and Physical Sciences, Heriot-Watt University, Edinburgh, U.K. (dr38@hw.ac.uk; G.Goussetis@hw.ac.uk)*
[2]*Department of Electrical Engineering, Group of Signal Theory and Communications, Universidad de Oviedo, 3320 - Gijón, Spain (arrebola@uniovi.es; jelofer@uniovi.es; mpino@uniovi.es)*
[3]*Information, Processing and Telecommunications Center, Universidad Politécnica de Madrid, 28040 - Madrid, Spain (jose.encinar@upm.es)*

***Abstract*— This contribution describes a general framework for the optimization of very large reflectarrays for space applications. It employs the generalized Intersection Approach with a series of techniques to accelerate computations. In particular, a machine learning technique is used to obtain a surrogate model of the reflectarray unit cell. Also, the gradient computation is accelerated by employing differential contributions on the radiated field. Computations may also be accelerated with the NUFFT employing a non-uniform grid in the spectral domain. Finally, instead of optimizing the crosspolar pattern, the XPD or XPI are optimized, improving both the antenna and algorithm performance. Relevant numerical examples are provided to show the capabilities of the proposed framework and acceleration techniques.**

I. Introduction

The requirements of antennas for satellite telecommunication missions are very stringent in terms of bandwidth and radiation patterns [1]. Although reflector antennas have been the classic solution for these applications they are bulky, expensive and difficult to fold and deploy. Other concepts with advantages from the mechanical or electrical point of view have been studied in the last years. Planar antennas such as reflectarrays [2] or transmitarrays [3, 4] have been proposed for telecom missions, first for DBS (Direct Broadcast Satellite) missions [5, 6] and more recently as mutibeam antennas [7]. They are interesting from a mechanical point of view while significant improvements in bandwidth, which has traditionally been a key concern, have been recently achieved [8]. However, the requirements in terms of beam shaping and crosspolar level call for synthesis and optimization techniques in the design process that do not compromise accuracy [9]. As a result, the design process can be difficult to manage or even be considerably slow since the reflectarray is made up of thousands of elements, each one with one or several degrees of freedom to optimize, and high accuracy implies the use of accurate and typically slow analysis techniques.

In this contribution, an efficient technique for the optimization of large reflectarray antennas is proposed, discussed and validated with several test cases, with application in radiation pattern synthesis and crosspolar reduction. The technique is based on the generalized Intersection Approach framework [10] using the Levenberg-Marquard Algorithm (LMA) [11] as backward projector. The accuracy of the approach is ensured by the analysis of the reflectarray elements through a full-wave analysis technique based on spectral domain Method of Moments assuming Local Periodicity (MoM-LP) [12] and using the First Principle of Equivalence in electromagnetics for the evaluation of the radiation pattern. Starting from this framework, several improvements are introduced involving the calculation of the radiated field, the gradient computation, the modelling of the reflectarray elements and the definition of the cost function in order to greatly speed up the technique to handle very large reflectarrays comprised of several thousands of elements. In addition, the convergence of the algorithm is also improved and as a consequence the performances of the final antenna. Several test cases on satellite telecommunication missions are considered, including very large multibeam reflectarrays and shaped-beam reflectarrays for DBS missions with improved XPD and XPI levels.

II. Optimization Framework

The optimization framework is based on the generalized Intersection Approach (IA) presented in [10] and particularized for the crosspolar optimization of reflectarray antennas in [9]. Figure 1 shows the flowchart of the algorithm. Starting from the initial layout, it applies iteratively two operations: the forward and the backward projection. In the forward projection, the radiation pattern is calculated and trimmed according to some specification templates given in the form of upper and lower masks. Then, in the backward projection the trimmed pattern is employed as reference for a local optimization procedure using the LMA.

The technique presented in [9] employed a MoM-LP as analysis technique to obtain an accurate prediction of the electromagnetic behaviour of the unit cell. However, this caused the algorithm to be relatively slow and to only be

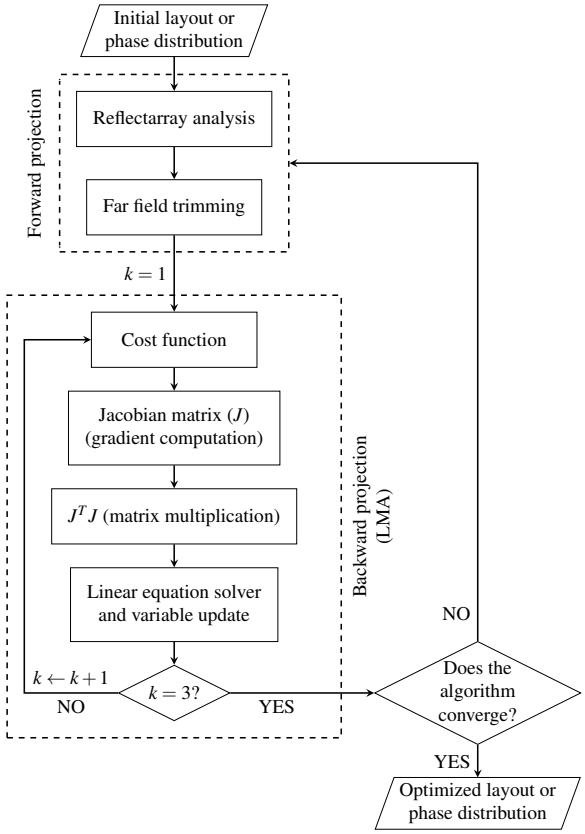

Figure 1: Flowchart of the generalized Intersection Approach particularized for the optimization of reflectarray antennas.

practical for very large reflectarrays using workstations. In any case, the good convergence properties of the generalized IA [13, 14] allow to handle tens of thousands of optimizing variables while obtaining good results. This is done by minimizing the number of local minima by working with the squared field amplitude (or equivalently the gain) and performing the optimization in several steps, incrementing the number of optimizing variables as suggested in [10].

From a computational point of view, [9] introduced a number of strategies to accelerate computations of the main building blocks of the LMA in the backward projection (see Figure 1), since the computing time of the forward projection is negligible. First, the computation of all building blocks is parallelized, the cost function and Jacobian matrix using OpenMP and the matrix multiplication and linear equation solver using the Intel MKL libraries. In addition, the number of calls to the MoM-LP routine in the Jacobian matrix computation are minimized since only one element per column is modified when the derivative is evaluated using finite differences. Also, as linear equation solver the Cholesky factorization is used, since it is the fastest exact solver available. Further details may be consulted in [9, 11]. Despite the computational improvements introduced to the generalized IA, there is still room for further improvements which will be addressed next.

III. Further Improvements in Analysis and Optimization of Reflectarrays

This section introduces two new improvements for a faster analysis of reflectarray antennas based on Support Vector Machines (SVMs) and the Non-Uniform FFT (NUFFT) with direct application in the optimization procedure; plus two new techniques specifically focused on accelerating and improving the optimization algorithm, namely, differential contributions to the radiated field (DFC) and the direct optimization of the crosspolar discrimination (XPD) and isolation (XPI).

A. Surrogate Model with Support Vector Machines

Although the full-wave MoM-LP employed [12] is considerably faster than other general purpose full-wave commercial solutions, it makes the optimization slow since the MoM-LP routine is called thousands of times. Some approaches to accelerate the simulation of the unit cell consist on the use of databases, artificial neural networks or Support Vector Machines (SVM). The latter is the approach followed in this work.

SVMs are automatic and supervised learning algorithms which are used to solve regression and classification problems. In the present case, the SVM regression characteristics are adapted to seek a surrogate model of the unit cell. A complete description of the SVM theory background and training strategies may be found in [15]. Only the basic features will be described here for completeness.

For a given training set of inputs and outputs, $S = \{\vec{x}_i, y_i\}_{i=1,2,\ldots,N_r}$, with $\vec{x}_i \in \chi \subseteq \mathbb{R}^L$ and $y_i \in \mathbb{R}$, the SVM is used to obtain a function f which estimates the output $\tilde{y}$ that corresponds to a new input $\vec{x}$ as:

$$\tilde{y} = f(\vec{x}), \tag{1}$$

where f follows the expression:

$$f(\vec{x}) = b + \sum_{i=1}^{N_s} \left[\left(\alpha_i^- - \alpha_i^+ \right) K(\vec{x}_i, \vec{x}) \right], \tag{2}$$

and b is known as the offset, N_s is the total number of support vectors, α_i^+ and α_i^- are the optimal Lagrange multipliers, and K is the kernel function, which in the present case is a Gaussian kernel:

$$K(\vec{x}, \vec{x}') = \exp\left(-\gamma \|\vec{x} - \vec{x}'\|^2\right), \tag{3}$$

where $\|\cdot\|$ is the Euclidean norm and γ a tunable parameter.

The obtained function f in (2) minimizes a regularized risk functional that accounts for the empirical errors (weighted by a tunable parameter C) and for the flatness of f. When the flatness is maximized, f has good generalization properties. On the other hand, the empirical errors account for how well it fits the training samples. Thus C provides a trade-off between the two. The parameters γ and C determine the shape of function f and must be carefully selected through a grid search in the (C, γ) plane [15].

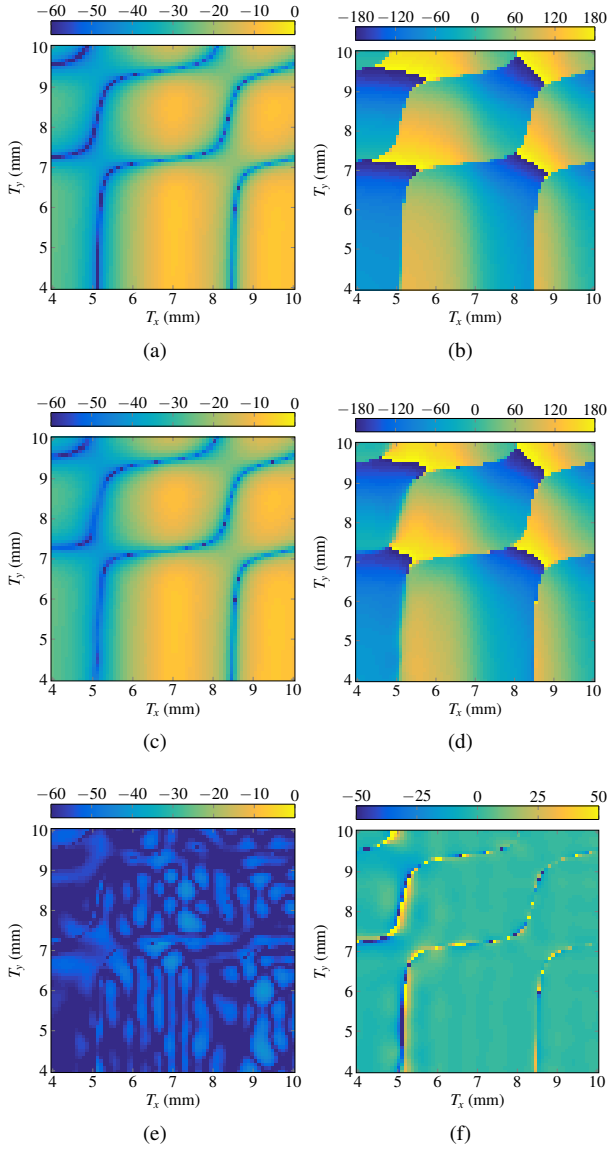

Figure 2: For the reflection coefficient ρ_{yx} with $(\theta = 35°, \varphi = 35°)$, comparison between (a), (b) the MoM-LP simulation and (c), (d) SVM simulation for the (a), (c) magnitude in dB and (b), (d) phase in degrees. Difference of the (e) magnitude is in dB and of the (f) phase in degrees.

The SVM is used to obtain the surrogate model of the matrix of reflection coefficients $\mathbf{R}^{mn}$ for the unit cell described in [9]. As in [15], only two geometric variables are considered, T_x and T_y. Due to the low losses and good behaviour of the direct coefficients ρ_{xx} and ρ_{yy}, the error is very low. It is more difficult to obtain a good surrogate model of the cross-coefficients. Figure 2 shows a comparison in magnitude and phase of the cross-coefficient ρ_{yx} for an oblique angle of incidence $(\theta = 35°, \varphi = 35°)$. The magnitude difference is very low, always below -40 dB. However, the phase difference shows high values where there are abrupt changes which the SVM simulation tends to soften. In any case, the mean absolute deviation (MAD) is 4° for this case, and 4.5°for the phase of ρ_{xy}, which are considered very low values for a cross-coefficient (for the phases of ρ_{xx} and ρ_{yy} the MAD is lower than 0.6°). The mean relative error of the training for all reflection coefficients is -33 dB following [15], which will provide a high degree of accuracy in the predicted radiation patterns, as it will be shown later.

Table 1: Computational time study for an FFT resolution of 512×512 (44 748 points considered in the optimization) and 7 993 optimizing variables. All values are in seconds.

Tool	Cost function	Jacobian	$\mathbf{J}^T\mathbf{J}$	Solver
MoM-LP	30.08	90.73	17.66	1.20
SVM	0.22	48.30	17.73	1.21

Apart from a high degree of accuracy with regard to the MoM-LP simulations, the SVM considerably accelerates the computation of the $\mathbf{R}^{mn}$ matrix. For instance, for a reflectarray comprised of 5 180 elements for DBS, it took 116.70 s to MoM-LP while for the SVM the computation of the reflection coefficient matrices only took 34.8 ms, which supposes a speed-up factor of 3350. This acceleration factor corresponds to the computation of $\mathbf{R}^{mn}$. When applied to the design of the reflectarray layout, using MoM-LP it took 4 655.98 s (1 h and 18 min), while using SVM it took only 8.24 s, which correspond to a speed-up factor of 565.

Finally, Table 1 shows the impact of using SVM in the optimization algorithm. The computation of the cost function is accelerated by a factor greater than 130. It is smaller than the layout design speed-up since the cost function also requires the computation of several spectrum functions with the FFT to obtain the far field, which are not accelerated by the SVM. On the other hand, the Jacobian matrix computation takes close to half the time with SVM than with MoM-LP. However, the acceleration is very small in this case. The reason is that each column of the Jacobian substitutes one call to the MoM-LP routine for a SVM simulation. However, each column still requires the computation of eight spectrum functions for dual-polarized reflectarray antennas, and since they are not accelerated by the SVM, it penalizes the computation speed.

B. Acceleration of Far Field Computation with Adaptive Grid and NUFFT

The most time consuming operation when computing the radiation pattern of an aperture is the computation of the spectrum functions, which take the form [16]:

$$P(u,v) = K \sum_{i=1}^{N} \left[E_i(x_i, y_i) \exp\left(jk_0 \left(u x_i + v y_i \right) \right) \right], \quad (4)$$

where E_i is one generic component of the tangential field, (x_i, y_i) are the coordinates of the i-th sample or element,

k_0 the free-space wavenumber, K the unit cell pattern [16] and $u = \sin\theta\cos\varphi$, $v = \sin\theta\sin\varphi$.

When $P(u,v)$ is efficiently computed by means of the FFT, it reduces the time cost from $\mathcal{O}(NM)$ of the direct evaluation of (4) to $\mathcal{O}(M\log M)$, where M the number of points in the (u,v) grid where the far field is computed. However, the use of the FFT might present some limitations, especially regarding new applications, such as multibeam, where very large reflectarrays, with narrow beams are being studied. For instance, the reflectarray proposed in [7] has more than 20 000 elements with a beam spacing smaller than 0.6°. Thus, high resolution in the spectral domain (u,v) is required to correctly characterize the main beam, including gain, side lobes, etc.

Using the FFT imposes a fixed (u,v) grid [2], whose memory footprint grows exponentially with the resolution. Typically, the FFT grid is of the form $M = 2^n \times 2^n$, with $n \in \mathbb{N}$ controlling the resolution. This means that for highly directive antennas, memory usage might become prohibitive. A solution could be to compute the spectrum functions by brute force in $\mathcal{O}(NM)$ only in the region of interest with high resolution. However, due to the high number of elements, it is computationally very inefficient. One possible solution to this problem is the use of the Non-Uniform FFT (NUFFT).

The NUFFT is a generalization of the FFT that allows for non-uniform grids in both domains, the physical domain (x,y) (reflectarray aperture) and the spectral domain. Thus, it reduces the time cost of evaluating (4) from $\mathcal{O}(NM)$ to $\mathcal{O}(M\log M)$. However, although the computational complexity scaling is the same as the FFT, the NUFFT is slower and precision dependent. There is a parameter ψ that controls the accuracy of the obtained results. For the two-dimensional case, a more accurate description of its time complexity is [16]:

$$\mathcal{O}(M\log M + M\log^2\psi^{-1}), \tag{5}$$

where ψ can be set to obtain an arbitrary low error at the expense of slower computations.

To evaluate the technique, a multibeam antenna [7] with high resolution and very narrow beamwidth is considered. The reflectarray is elliptical with 247×241 elements in its main axes, and with a total of 46 751 unit cells. The working frequency is 19.7 GHz and the periodicity is $7.5\times7.5\,\text{mm}^2$. The feed is placed at $(-661, 0, 2726)$ mm from the reflectarray center and is modelled as a $\cos^q\theta$ function with $q = 24$. For this example, the NUFFT is employed to efficiently compute the points only in the principle plane. This is equivalent to perform a 2D to 1D transformation. In practise, the spectral domain is considered a rectangle with a dimension smaller than the distance between two adjacent samples.

To test the technique, the main cut will be non-uniform: high resolution will be imposed around the main beam in $u \in [0.15, 0.30]$, with a step of 2^{-14}; a medium resolution in $u \in [0, 0.15] \cup [0.30, 0.45]$ for the closest side lobes, with a step of 2^{-12}; and low resolution in the rest of the

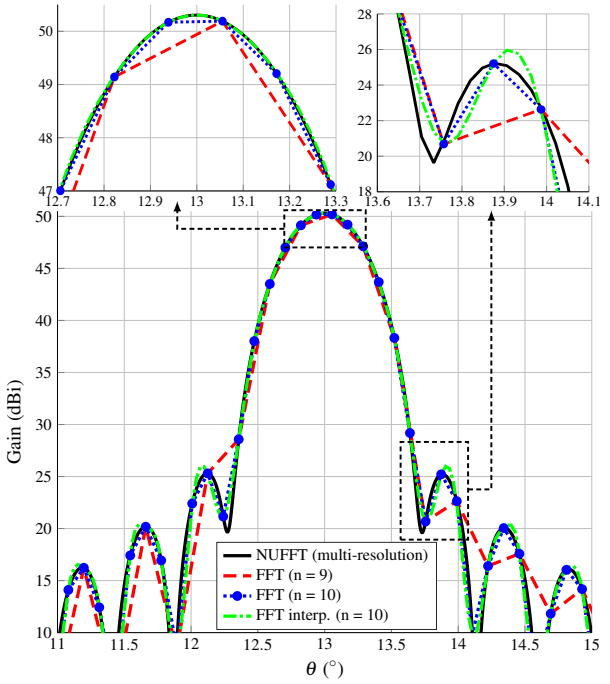

Figure 3: Comparison of the main cut computed in an adaptive grid with multi-resolution using the NUFFT and two typical values of n using the FFT plus spline interpolation.

cut for the farthest side lobes, with a step of 2^{-10}. (Due to the relation between θ and u for $v = 0$, the discretization in the corresponding intervals in θ is non-uniform.) Figure 3 shows the computed cut around the main beam for the NUFFT and two typical values of n for the FFT plus a spline interpolation of a FFT simulation. As shown, the NUFFT provides high resolution while the memory usage is negligible (< 1 MB). To achieve the same angular resolution with the FFT, a value $n = 14$ is needed, since the step between adjacent points in the main beam is 2^{-14} for the NUFFT. With that resolution, the FFT would have a memory footprint of 4 GB per spectrum function. The points computed by the FFT with $n = 9, 10$ lie exactly on the curve computed by the NUFFT, but do not provide enough density of points for a proper representation, including the value of maximum gain. When using the spline interpolation for the FFT with $n = 10$, side lobes are not well predicted, and worse results were obtained for the intepolation for the FFT with $n = 9$.

A direct evaluation may be used to compute the main cut. The computation of the spectrum functions in the visible region is slower using this method, but the number of points in a single cut is considerably lower. A time study was performed comparing the direct evaluation and the NUFFT and it is shown in Figure 4. Despite the reduction in the number of points, the direct evaluation is still slower due to the large amount of reflectarray elements, and is only faster than the NUFFT for $\xi = 10^{-8}$ in the case with the smallest number of points in the tested cut.

This technique may be used to reduce the total num-

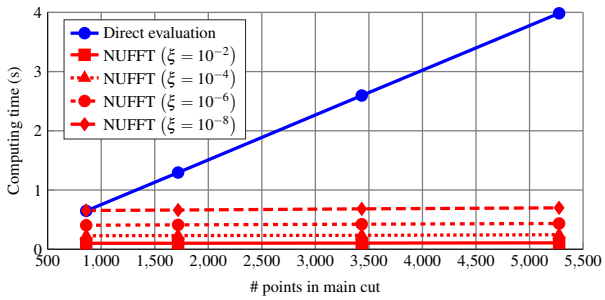

Figure 4: Comparison of computing time between the direct evaluation and NUFFT when computing the radiation pattern only in the main cut.

ber of points where the far field is computed (M), effectively reducing the size of the Jacobian matrix leading to a faster Jacobian matrix evaluation and matrix multiplication ($J^T J$).

C. Accelerating Gradient Computation with Differential Contributions

Using the SVM greatly accelerated the cost function, as shown in Table 1. However, the Jacobian matrix computation, though faster with the SVM than with MoM-LP, did not show a good enough speed-up factor since the computation of the far field starting from the tangential field is not accelerated, although it may be accelerated using an adaptive grid with the NUFFT. However, the lying issue with the gradient computation is that when performing a direct optimization of the layout, there is no analytical expression relating the optimizing variables and the cost function that it is easy to derive analytically, as opposed to the POS, which can be done either for near field or far field. Thus, finite differences must be used to compute the derivatives. However, the gradient computation may be accelerated by employing the technique of differential contributions to the radiated field.

The Jacobian matrix may be formed with the gradient of a multidimentional scalar cost function of the form:

$$\nabla f(\vec{r},\bar{\xi}) = \left(\frac{\partial f(\vec{r},\bar{\xi})}{\partial \xi_1}, \cdots, \frac{\partial f(\vec{r},\bar{\xi})}{\partial \xi_i}, \cdots, \frac{\partial f(\vec{r},\bar{\xi})}{\partial \xi_P} \right), \tag{6}$$

where $\bar{\xi} = (\xi_1, \ldots, \xi_i, \ldots, \xi_P)$ is a vector of P optimizing variables and $\vec{r} \in \{\vec{r}_1, \ldots, \vec{r}_t, \ldots, \vec{r}_M\}$ an observation point where the radiated field is computed. Since there is no analytical expression to calculate each derivative, they are computed using finite differences. Using a backward lateral difference the derivative is:

$$\frac{\partial f(\vec{r},\bar{\xi})}{\partial \xi_i} = \frac{f(\vec{r},\bar{\xi}) - f(\vec{r},\bar{\xi} - h\hat{e}_i)}{h} + \mathcal{O}(h), \tag{7}$$

where h is a small positive scalar [11], and $\hat{e}_i$ is the ith unit vector such that:

$$\bar{\xi} - h\hat{e}_i = (\xi_1, \ldots, \xi_i - h, \ldots, \xi_P). \tag{8}$$

For the computation of the derivative by means of (7), the cost function $f(\vec{r},\bar{\xi})$ depends on the radiated field $\vec{E}(\vec{r},\bar{\xi})$ and it is common to all P derivatives in (6), so it only needs to be computed once. On the other hand, $f(\vec{r},\bar{\xi} - h\hat{e}_i)$ depends on $\vec{E}(\vec{r},\bar{\xi} - h\hat{e}_i)$, and it is computed for each derivative. Since the reflectarray analysis assumes local periodicity, the modification of one element (variable) does not affect the others, and the perturbed field may be computed with the differential contribution:

$$\vec{E}(\vec{r},\bar{\xi} - h\hat{e}_i) = \vec{E}(\vec{r},\bar{\xi}) + \Delta\vec{E}(\vec{r},\xi_i), \tag{9}$$

where $\Delta\vec{E}(\vec{r},\xi_i)$ is the differential contribution to the radiated field produced by the reflectarray element depending on variable i:

$$\Delta\vec{E}(\vec{r},\xi_i) = \vec{E}(\vec{r},\xi_i - h) - \vec{E}(\vec{r},\xi_i). \tag{10}$$

Thanks to the linearity of Maxwell's equations, there exists a linear relation between the field at the aperture and the radiated field (either near or far field). If we denote by $\vec{E}_{\text{ref},k}(\vec{r}'_k,\xi_i)$ the reflected tangential field of element k at location $\vec{r}'_k$, with $k = 1,\ldots,N$ and depending on variable ξ_i, (10) can be expressed writing the radiated field as a function of the tangential field:

$$\Delta\vec{E}(\vec{r},\xi_i) = \vec{E}(\vec{r},\vec{E}_{\text{ref},k}(\vec{r}'_k,\xi_i - h)) - \vec{E}(\vec{r},\vec{E}_{\text{ref},k}(\vec{r}'_k,\xi_i)). \tag{11}$$

Since the radiated field is linear with respect to the tangential field:

$$\Delta\vec{E}(\vec{r},\xi_i) = \vec{E}(\vec{r},\Delta\vec{E}_{\text{ref},k}(\vec{r}'_k,\xi_i)), \tag{12}$$

where:

$$\Delta\vec{E}_{\text{ref},k}(\vec{r}'_k,\xi_i) = \vec{E}_{\text{ref},k}(\vec{r}'_k,\xi_i - h) - \vec{E}_{\text{ref},k}(\vec{r}'_k,\xi_i). \tag{13}$$

Thus, (12) indicates that to compute one derivative, only the differential contribution of one element is necessary. In practise, this means that, starting from the tangential field, the time cost of computing the far field is reduced from $\mathcal{O}(M \log M)$ when using the (NU)FFT to $\mathcal{O}(M)$ using the Differential Contributions (DFC) technique in the computation of each derivative [17].

As an example, the technique of DFC was implemented for POS using the generalized IA detailed in [18] and compared, for a periodic reflectarray, with the computation of the far field with the NUFFT, the FFT and the analytic derivative. Figure 5 shows the measured computing time comparing different techniques. As it can be seen, the DFC is faster than the FFT, NUFFT and even the analytic derivative for the computation of the Jacobian matrix (gradient). In this case, the analytic derivative and DFC present the same time complexity scaling, but the DFC requires fewer operations inside the loop sweeping all M points. The mean speed-up of the DFC is 94.2%, 56.9% and 29.8% with regard to the use of the NUFFT, FFT and analytic derivative, respectively.

The DFC technique was also implemented for the direct optimization of the layout with both MoM-LP and SVM. Table 2 shows the updated results when using the DFC. The Jacobian matrix computation is substantially accelerated by the combination of the SVM and DFC. By itself,

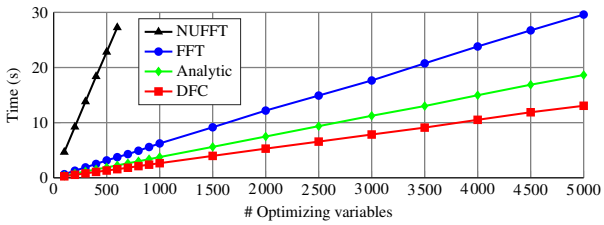

Figure 5: Measured computing time of the Jacobian matrix evaluation for the far field with the FFT, NUFFT ($\psi = 10^{-2}$), Differential Contributions (DFC) and analytic derivative for a POS considering different numbers of optimizing variables using a UV grid of 512×512 points and computations parallelized with 20 threads.

Table 2: Computational time study for an FFT resolution of 512×512 (44 748 points considered in the optimization) and 7 993 optimizing variables. All values are in seconds.

Tool	Cost function	Jacobian	$\mathbf{J^T J}$	Solver
MoM-LP	30.08	90.73	17.66	1.20
MoM-LP + DFC	30.08	61.77	19.23	1.22
SVM	0.22	48.30	17.73	1.21
SVM + DFC	0.22	4.06	18.77	1.22

the DFC technique accelerates the computation of the Jacobian, going from taking almost 91 seconds to approximately 62 seconds. However, when combining SVM and DFC the gradient computation is accelerated more than one order of magnitude, reaching a speed up factor of 22.3 in the present case.

D. XPD and XPI Optimization

The usual approach to perform crosspolar optimization is to impose some requirements directly on the crosspolar pattern with the aim of reducing it [9]. However, in some space applications, such as DBS, the figure of merit for cross-polarization performance is the crosspolar discrimination (XPD) or the crosspolar isolation (XPI). If the crosspolar pattern is optimized, the XPD and XPI are optimized indirectly, providing suboptimal results. Thus, it is proposed to directly optimize the XPD and XPI in order to improve the performance of the antenna. This is achieved by a proper redefinition of the backward projector presented in [9], substituting the crosspolar templates by XPD and XPI templates.

The crosspolar discrimination (XPD) is defined, in linear scale, as the ratio point by point of the copolar and crosspolar gain:

$$\mathrm{XPD}(u,v) = G_{\mathrm{cp}}(u,v)/G_{\mathrm{xp}}(u,v), \quad \forall\,(u,v) \in \Omega, \quad (14)$$

where Ω is the coverage zone. For the present case, the worst XPD value is considered in the optimization, corresponding to its minimum:

$$\mathrm{XPD}_{\mathrm{min}} = \min\{\mathrm{XDP}(u,v)\}. \quad (15)$$

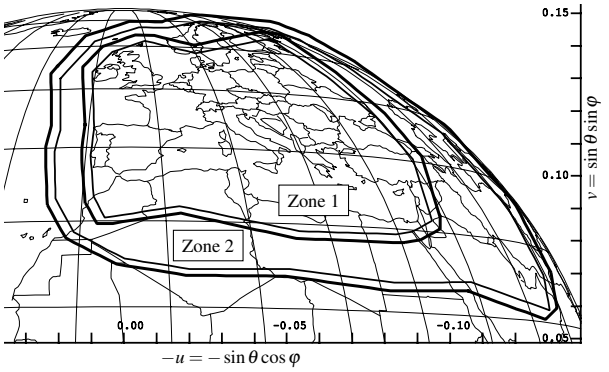

Figure 6: Europe footprint with two coverage zones for DBS application with (u,v) coordinates in the antenna coordinate system.

On the other hand, the crosspolar isolation (XPI) is defined in linear scale as follows:

$$\mathrm{XPI} = \frac{\min\{G_{\mathrm{cp}}(u,v)\}}{\max\{G_{\mathrm{xp}}(u,v)\}}, \quad (u,v) \in \Omega. \quad (16)$$

The goal of the optimization algorithm is to maximize the $\mathrm{XPD}_{\mathrm{min}}$ and XPI values for each coverage zone. Thus, only minimum templates are imposed in the backward projector. If $T_{\mathrm{min}\{\mathrm{XPD}_{\mathrm{min}}\}}$ and $T_{\mathrm{min}\{\mathrm{XPI}\}}$ are the minimum templates, the following condition should be met:

$$\begin{aligned} T_{\mathrm{min}\{\mathrm{XPD}_{\mathrm{min}}\}} &\leq \mathrm{XPD}_{\mathrm{min}}, \\ T_{\mathrm{min}\{\mathrm{XPI}\}} &\leq \mathrm{XPI}. \end{aligned} \quad (17)$$

Given the formulation of the backward projector in [9], the crosspolar templates are substituted with (17). The copolar templates are maintained to keep the copolar pattern within specifications while the cross-polarization performance of the antenna is improved.

IV. Optimization of a Very Large Reflectarray

A. Antenna Specifications

The considered reflectarray is elliptical, has a total of 4 068 elements in a regular grid with 74 and 70 cells in its main axes. The periodicity of the unit cell is 14 mm × 14 mm and the working frequency is 11.85 GHz. The feed is modeled as a $\cos^q\theta$ function with $q = 23$, generating an illumination taper of −17.9 dB. Also, the feed is placed at $(-358, 0, 1070)$ mm, while the whole antenna is on a satellite in geostationary orbit at 10° E longitude. In addition, one SVM is trained per angle of incidence. A total of 136 pairs of (θ, φ) angles are obtained, which are further reduced to 68 pairs using symmetries. Finally, Figure 6 shows the contour requirements for Europe with two coverage zones. The copolar requirements are 28.5 dBi for zone 1 and 25.5 dBi for zone 2. The optimization will be carried out in dual-linear polarization using the same template specifications for both polarizations.

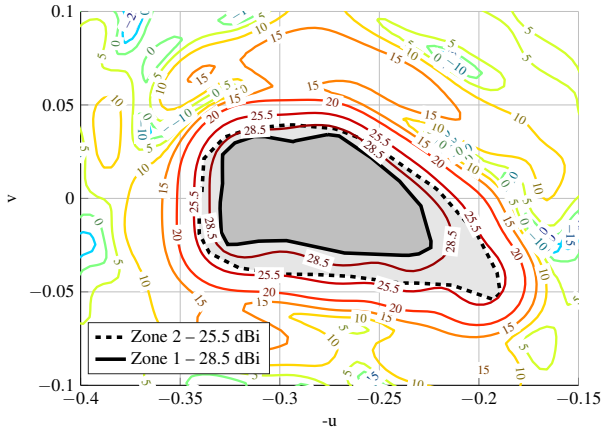

(a)

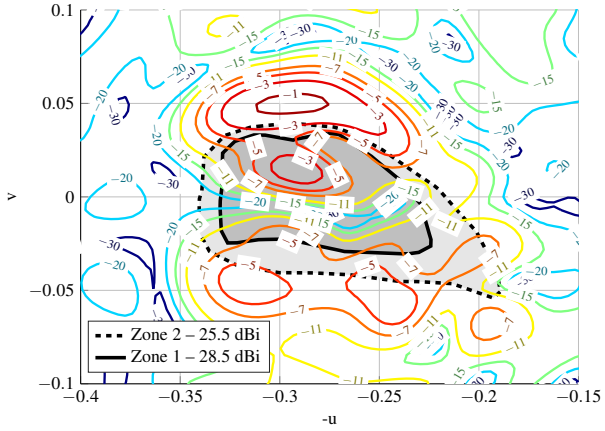

(b)

Figure 7: Radiation pattern in dBi for polarization X obtained after the POS. (a) Copolar. (b) Crosspolar.

B. Results

The starting point for the crosspolar optimization is a layout obtained after a POS with the generalized IA [18]. The simulated radiation pattern for polarization X is shown in Figure 7 and perfectly complies with the specifications for the copolar pattern. Similar results were obtained for polarization Y.

For the crosspolar optimization, three different strategies are compared: the optimization of the crosspolar pattern, the XPD_{min} and the XPI. The goal is to show that directly optimizing the figure of merit for cross-polarization performance achieves better results. The three approaches were tested with the generalized IA, which was run for 80 iterations until the error stagnated. The final results are summarized in Table 3, which also includes the starting point corresponding to the pattern of Figure 7 and the minimum copolar gain for both coverage zones and linear polarizations. As it can be seen, the XPD_{min} and XPI are effectively improved in all cases. However, directly optimizing their values provides better results. For instance, for zone 1 the XPD_{min} reaches a value of 35.10 dB when optimizing the crosspolar pattern, but it improves to 39.64 dB and 39.53 dB when optimizing the XPD_{min} and XPI, respectively, in polarization X. This supposes an increment of more than 4 dB with the new proposed strategy over the usual approach, and more than 8 dB over the starting point (31.46 dB). This improvement occurs for both polarizations and both coverage zones as shown in Table 3.

V. Conclusions

This contribution has presented a series of techniques for the improvement of a general framework for the optimization of very large reflectarrays for space applications. They include the use of SVMs to obtain a fast and accurate surrogate model to substitute the MoM-LP tool in the computations, accelerating the analysis and layout design more than three and two orders of magnitude, respectively. Also, the technique of differential contributions on the far field allows to substantially accelerate the gradient computation in local-search algorithms, including also POS. The use of the NUFFT allows to have a non-uniform spectral grid with high resolution in the areas of interest and low resolution elsewhere, reducing both computing time and memory usage with regard to the FFT. Finally, the direct optimization of the XPD or XPI allows to improve the cross-polarization performance of the optimize antenna with regard to the optimization of the crosspolar pattern. These techniques were demonstrated with the optimization of a large reflectarray with European coverage, showing promising results.

Acknowledgments

This work was supported in part by the European Space Agency (ESA) under contract ESTEC/AO/1-7064/12/NL/MH; by the Ministerio de Ciencia, Innovación y Universidades under project TEC2017-86619-R (ARTEINE); by the Ministerio de Economía, Industria y Competitividad under project TEC2016-75103-C2-1-R (MYRADA); by the Gobierno del Principado de Asturias through Programa “Clarín” de Ayudas Postdoctorales / Marie Courie-Cofund under project ACA17-09.

References

[1] W. A. Imbriale, S. Gao, and L. Boccia, Eds., *Space Antenna Handbook*. Hoboken, NJ, USA: John Wiley & Sons, 2012.

[2] J. Huang and J. A. Encinar, *Reflectarray Antennas*. Hoboken, NJ, USA: John Wiley & Sons, 2008.

[3] S. A. Matos, E. B. Lima, J. S. Silva, J. R. Costa, C. A. Fernandes, N. J. G. Fonseca, and J. R. Mosig, “High gain dual-band beam-steering transmit array for satcom terminals at Ka-band,” *IEEE Trans. Antennas Propag.*, vol. 65, no. 7, pp. 3528–3539, Jul. 2017.

[4] K. T. Pham, R. Sauleau, E. Fourn, F. Diaby, A. Clemente, and L. Dussopt, “Dual-band transmitarrays with dual-linear polarization at Ka-band,” *IEEE Trans. Antennas Propag.*, vol. 65, no. 12, pp. 7009–7018, Dec. 2017.

[5] J. A. Encinar, L. S. Datashvili, J. A. Zornoza, M. Arrebola, M. Sierra-Castaner, J. L. Besada-Sanmartin,

Table 3: Results of the direct optimization using SVM of a reflectarray antenna with a European footprint with two coverage zones comparing different strategies: the usual approach of optimizing the crosspolar component of the radiation pattern (XP opt.) and the new strategy of directly optimizing the figure of merit (XPD_{min} opt. and XPI opt.). Values of CP_{min} are in dBi and values of XPD_{min} and XPI are in dB.

	Zone 1 (28.5 dBi)						**Zone 2 (25.5 dBi)**					
	Pol. X			**Pol. Y**			**Pol. X**			**Pol. Y**		
	CP_{min}	**XPD_{min}**	**XPI**	**CP_{min}**	**XPD_{min}**	**XPI**	**CP_{min}**	**XPD_{min}**	**XPI**	**CP_{min}**	**XPD_{min}**	**XPI**
Initial	29.29	31.46	30.13	29.32	31.46	30.13	26.03	27.98	25.92	26.03	28.45	26.44
XP opt.	29.30	35.10	34.57	29.26	35.60	33.38	26.27	31.85	31.11	26.31	31.63	31.07
XPD_{min} opt.	29.00	39.64	37.46	29.08	39.36	37.46	25.96	35.96	33.46	25.67	36.76	33.81
XPI opt.	29.04	39.53	39.25	29.01	40.32	39.00	25.80	34.78	34.49	26.06	36.29	35.75

H. Baier, and H. Legay, "Dual-polarization dual-coverage reflectarray for space applications," *IEEE Trans. Antennas Propag.*, vol. 54, no. 10, pp. 2827–2837, Oct. 2006.

[6] M. Zhou, O. Borries, and E. Jørgensen, "Design and optimization of a single-layer planar transmit-receive contoured beam reflectarray with enhanced performance," *IEEE Trans. Antennas Propag.*, vol. 63, no. 4, pp. 1247–1254, Apr. 2015.

[7] E. Martínez-de-Rioja, J. A. Encinar, A. Pino, B. González-Valdés, S. V. Hum, and C. Tienda, "Bifocal design procedure for dual reflectarray antennas in offset configurations," *IEEE Antennas Wireless Propag. Lett.*, 2018, in press.

[8] R. Florencio, J. A. Encinar, R. R. Boix, V. Losada, and G. Toso, "Reflectarray antennas for dual polarization and broadband telecom satellite applications," *IEEE Trans. Antennas Propag.*, vol. 63, no. 4, pp. 1234–1246, Apr. 2015.

[9] D. R. Prado, M. Arrebola, M. R. Pino, R. Florencio, R. R. Boix, J. A. Encinar, and F. Las-Heras, "Efficient crosspolar optimization of shaped-beam dual-polarized reflectarrays using full-wave analysis for the antenna element characterization," *IEEE Trans. Antennas Propag.*, vol. 65, no. 2, pp. 623–635, Feb. 2017.

[10] O. M. Bucci, G. D'Elia, G. Mazzarella, and G. Panariello, "Antenna pattern synthesis: a new general approach," *Proc. IEEE*, vol. 82, no. 3, pp. 358–371, Mar. 1994.

[11] D. R. Prado, J. Álvarez, M. Arrebola, M. R. Pino, R. G. Ayestarán, and F. Las-Heras, "Efficient, accurate and scalable reflectarray phase-only synthesis based on the Levenberg-Marquardt algorithm," *Appl. Comp. Electro. Society Journal*, vol. 30, no. 12, pp. 1246–1255, Dec. 2015.

[12] R. Florencio, R. R. Boix, and J. A. Encinar, "Enhanced MoM analysis of the scattering by periodic strip gratings in multilayered substrates," *IEEE Trans. Antennas Propag.*, vol. 61, no. 10, pp. 5088–5099, Oct. 2013.

[13] A. Capozzoli, C. Curcio, A. Liseno, and G. Toso, "Fast, phase-only synthesis of aperiodic reflectarrays using NUFFTs and CUDA," *Progr. Electromagn. Res.*, vol. 156, pp. 83–103, 2016.

[14] D. R. Prado, M. Arrebola, M. R. Pino, and F. Las-Heras, "Improving convergence in crosspolar optimization of reflectarray antennas," in *11th European Conference on Antennas and Propagation (EuCAP)*, Paris, France, Mar. 19–24, 2017, pp. 100–103.

[15] D. R. Prado, J. A. López-Fernández, G. Barquero, M. Arrebola, and F. Las-Heras, "Fast and accurate modeling of dual-polarized reflectarray unit cells using support vector machines," *IEEE Trans. Antennas Propag.*, vol. 66, no. 3, pp. 1258–1270, Mar. 2018.

[16] D. R. Prado, M. Arrebola, M. R. Pino, and F. Las-Heras, "An efficient calculation of the far field radiated by non-uniformly sampled planar fields complying Nyquist theorem," *IEEE Trans. Antennas Propag.*, vol. 63, no. 2, pp. 862–865, Feb. 2015.

[17] D. R. Prado, A. F. Vaquero, M. Arrebola, M. R. Pino, and F. Las-Heras, "Acceleration of gradient-based algorithms for array antenna synthesis with far field or near field constraints," *IEEE Trans. Antennas Propag.*, 2018, in press.

[18] D. R. Prado, M. Arrebola, M. R. Pino, and F. Las-Heras, "Improved reflectarray phase-only synthesis using the generalized intersection approach with dielectric frame and first principle of equivalence," *Int. J. Antennas Propag.*, vol. 2017, pp. 1–11, May 2017.